Multifunctional Nano-Architecture for Biomedical Applications

Dongling Ma,[†] Jingwen Guan,[†] François Normandin,[‡] Stéphane Dénommée,[†] Gary Enright,[†] Teodor Veres,[‡] and Benoit Simard*[,†]

Steacie Institute for Molecular Sciences, National Research Council of Canada, 100 Sussex Drive, Ottawa, Ontario K1A 0R6, Canada, and Industrial Materials Institute, National Research Council of Canada, 75 de Mortagne Boulevard, Boucherville, Québec J4B 6Y4, Canada

Received September 14, 2005. Revised Manuscript Received February 3, 2006

A multifunctional architecture for biomedical applications has been developed by deliberately combining the useful functions of superparamagnetism, luminescence, and surface functionality into one material. Good control of the core−shell architecture has been achieved by employing a sol−gel synthesis. Superparamagnetic iron oxide nanoparticles are first coated with silica to isolate the magnetic core from the surrounding. Subsequently, the dye molecules are doped inside a second silica shell to improve photostability and allow for versatile surface functionalities. The architecture has been characterized by transmission electron microscopy, UV−vis absorption and emission spectroscopy, energy-dispersive X-ray spectroscopy, X-ray diffraction, and magnetometry. The hybrid nanoparticles exhibit improved superparamagnetic behavior over the as-received nanoparticles with a significant decrease in the blocking temperature. The architecture shows emission properties similar to those of the free dye molecules, suggesting that the first silica shell successfully prevents luminescence quenching by minimizing dye−magnetic core interactions.

Introduction

Magnetic nanoparticles have attracted a great deal of interest because of the properties arising from their finite size.[1−4] When the size of the particles decreases to below a critical value, generally less than 15 nm,[5] each nanoparticle becomes a single magnetic domain and exhibits remarkable superparamagnetic behavior when the temperature is above the so-called blocking temperature. Each individual nanoparticle has a large constant magnetic moment and behaves like a giant paramagnetic atom with a fast response to applied magnetic fields with negligible remanence and coercivity. These features make superparamagnetic nanoparticles very attractive for a broad range of biomedical applications because the risk of forming agglomerates is negligible at room temperature. Specifically, superparamagnetic nanoparticles have been found to be very useful in applications such as magnetic resonance imaging (MRI), targeted drug delivery, and magnetic separation.[6] For example, Zhao et al.[7] have demonstrated a highly efficient collection of a trace amount of DNA/mRNA from a mixture, down to femtomolar concentrations, by using such nanoparticles.

In bioanalysis, luminescence has been extensively exploited for detection and sensing. Dyes, especially organic dyes, have been widely used as signaling sources based on their emission properties. They have been proven to be quite useful but are still far from perfect as most of them suffer from severe photobleaching during the detection process.[8] In some cases, their low signaling intensity limits the achievable detection sensitivity.[9] To solve these issues, it is important to develop highly sensitive and photostable signaling materials. Great efforts have been made toward designing new labeling materials such as quantum dots,[10,11] resonance light scattering particles,[12] and dye-doped nanoparticles.[13,14] Of these materials, the last type appears most promising. By encapsulating thousands of dye molecules into one protective nanoparticle, excellent photostability and enhanced signal density are to be expected. Silica turns out to be a very good candidate for a protective matrix on account of its proven biocompatibility and stability in most of the biosystems. Moreover, silica chemistry is well-known, and standard chemistry protocols can be followed to conjugate various biomolecules to the silica surface, thus enabling silica-based particles to couple and label biotargets with selectivity and specificity. Tan et al.[13−16] have synthesized dye-doped silica nanoparticles with a reverse microemulsion technique and

* Corresponding author. Tel.: 1 613 990-0977. E-mail: benoit.simard@nrc-cnrc.gc.ca.
[†] Steacie Institute for Molecular Sciences.
[‡] Industrial Materials Institute.

(1) Sun, S.; Murray, C. B. *J. Appl. Phys.* **1999**, *85*, 4325.
(2) Park, J.-I.; Kim, M. G.; Jun, Y.-W.; Lee, J. S.; Lee, W.-R.; Cheon, J. *J. Am. Chem. Soc*. **2004**, *126*, 9072.
(3) Lee, Y.; Lee, J.; Bae, C. J.; Park, J.-G.; Noh, H.-J.; Park, J.-H.; Hyeon, T. *Adv. Funct. Mater*. **2005**, *15*, 503.
(4) Farrell, D.; Majetich, S. A.; Wilcoxon, J. P. *J. Phys. Chem. B* **2003**, *107*, 11022.
(5) Frenkel, J.; Dorfman, J. *Nature* **1930**, *126*, 274.
(6) Tartaj, P.; Morales, M. d. P.; Verdaguer, S. V.; G-Carreño, T.; Serna, C. J. *J. Phys. D: Appl. Phys.* **2003**, *36*, R182.
(7) Zhao, X.; T-Dytioco, R.; Wang, K.; Tan, W. *Anal. Chem.* **2003**, *75*, 3476.
(8) Fare, T. L.; Coffey, E. M.; Dai, H. Y.; He, Y. D. D.; Kessler, D. A.; Kilian, K. A.; Koch, J. E.; LeProust, E.; Marton, M. J.; Meyer, M. R.; Stoughton, R. B.; Tokiwa, G. Y.; Wang, Y. Q. *Anal.Chem.* **2003**, *75*, 4672.
(9) Zhou, X.; Zhou, J. *Anal. Chem.* **2004**, *76*, 5302.
(10) Maxwell, D. J.; Taylor, J. R.; Nie, S. M. *J. Am. Chem. Soc.* **2002**, *124*, 9606.
(11) Cao, Y. W. C.; Jin, R. C.; Mirkin, C. A. *Science* **2002**, *297*, 1536.
(12) Bao, P.; Frutos, A. G.; Greef, C.; Lahiri, J.; Muller, U.; Peterson, T. C.; Warden L.; Xie, X. Y. *Anal. Chem.* **2002**, *74*, 1792.
(13) Santra, S.; Zhang, P.; Wang, K.; Tapec, R.; Tan, W. *Anal. Chem.* **2001**, *73*, 4988.
(14) Zhao, X.; T-Dytioco R.; Tan, W. *J. Am. Chem. Soc.* **2003**, *125*, 11474.

10.1021/cm052067x CCC: $33.50 Published 2006 by the American Chemical Society
Published on Web 03/14/2006

demonstrated their great potential in biodetection. The signal intensity increased by 4 orders of magnitude.

In our work, we are combining two useful functions, superparamagnetism and luminescence, along with an easily conjugated silica surface into one multifunctional nanoarchitecture. The direct attachment of dye molecules to magnetic nanoparticles results in luminescence quenching. To avoid this problem, the first silica shell must cover the magnetic cores to isolate them from the dye molecules and the surrounding. Subsequently, the dye molecules are doped inside a second silica shell to concentrate the emission signal and enhance the photostability. Herein, the synthesis and detailed structural, magnetic, and optical characterizations of this double-shell structure are presented.

Experimental Section

Materials. Water-soluble iron oxide nanoparticles (Fe_xO_y) with a reported average size of 10 nm and bearing the commercial label ferrofluid EMG 304 were obtained from Ferrotec Corporation (U.S.A.). Tris(2,2′-bipyridine) ruthenium(II) chloride (Rubpy) was purchased from Alfa Aesar, Johnson Matthey Company. Tetraethoxysilane (TEOS) and 3-aminopropyltriethyoxysilane (APS) were both ordered from Gelest, Inc. Ammonium hydroxide (NH_4OH, 28−30 wt %), high purity 2-propanol, tetrahydrofuran (THF), ethyl acetate, and hexane were obtained from EMD Chemicals, Inc. 1-Pyrenemethanol, sodium hydride (NaH, 60 wt %), triethylamine (Et_3N), 1,11-dibromoundecane, silica 60, toluene, and acetone were all ordered from Sigma-Aldrich Co. Silver nitrate ($AgNO_3$), petroether (bp 30−65 °C), and cyclohexane were purchased from Strem Chemicals, Inc., Anachemia Canada, Inc., and BDH, Inc., respectively. All chemicals were used directly without further purification. Water was purified with a Millipore Q-guard 2 purification system (Millipore Corporation). Only purified water (18 MΩ·cm) was used in the experiments.

Preparation of Core−Shell Nanoparticles. Before combining the dye molecules with the magnetic cores, a shell of dye-free silica (i.e., the first silica shell) has to be coated onto the magnetic particles to form the $Fe_xO_y@SiO_2$ structure. This shell plays the role of minimizing core−core and core−surroundings interactions as well as preventing emission quenching through core−dye interactions. The coating process has been carried out in an aqueous medium via the modified Stöber method.[17,18] The as-received ferrofluid EMG 304 was first diluted with high purity water to a particle concentration of about 10^{14} per mL. This primary stock solution was used to prepare subsequent solutions. The following coating conditions were typically used for the synthesis reaction leading to the core−shell particles with our interested shell thickness (10−15 nm) and morphology. First, 20 mL of water was added to 2.4 mL of the primary stock solution, and the resulting dispersion was sonicated in a Branson 5510 sonication bath for 30 min. At the same time, 36 μL of TEOS was dissolved into 160 mL of 2-propanol, and the freshly prepared silane solution was added under vigorous stirring to 22.4 mL of the previously sonicated dispersion. Next, 2.4 mL of NH_4OH was added to the reaction mixture. The resulting dispersion was mechanically stirred for at least 5 h at room temperature. The formed $Fe_xO_y@SiO_2$ nanoparticles were centrifuged, collected, and washed for magnetic, structural, or other characterizations.

To form the luminescent core−shell structure, that is, $Fe_xO_y@SiO_2@SiO_2$−Rubpy, the as-prepared $Fe_xO_y@SiO_2$ dispersion was used directly. The fresh silane solution was prepared by adding 67 μL of TEOS to 15 mL of 2-propanol. The fresh dye solution was prepared by dissolving about 4.5 mg of Rubpy to 10 mL of 2-propanol and 5 mL of water. The synthesis was accomplished by simultaneous dropwise addition of the above two solutions to the coating mixture. The entire addition process took about 2 h. The reactor was covered with aluminum foil, and the reaction was allowed to proceed for at least 12 h. The particles were then collected by centrifugation and repeatedly washed with water to remove unreacted Rubpy molecules before performing the photophysical measurements. A simpler method in which TEOS and Rubpy were added quickly within 1 min was also tried.

Synthesis of Luminescent Silica Nanoparticles. Similar procedures were employed to prepare the Rubpy-doped silica nanoparticles. Thirty-six (36) microliters of TEOS and 8 mg of Rubpy were added to 160 mL of 2-propanol and 20 mL of water. The particle synthesis was initiated by adding 2.4 mL of NH_4OH into the mixture under vigorous stirring. The reaction was allowed to proceed for at least 5 h. The particles were collected by centrifugation and washed with water in the same way as described earlier.

Attachment of Pyrene Groups to the Surface of $Fe_xO_y@SiO_2$ and Fe_xO_y Particles. To covalently attach the pyrene (Py) group to the $Fe_xO_y@SiO_2$ surface, 1-pyrenemethanolate sodium was first reacted with 1,11-dibromoundecane to form 1-pyrenemethoxybromoundecane (Br−Py), which was then coupled to APS to form APS−Py through a nucleophilic substitution reaction between the Br and NH_2 groups. A detailed description of the preparation of Br−Py is as follows. A suspension of 0.3 g of NaH in 10 mL of THF was mixed with 0.84 mmol of 1-pyrenemethanol in 5 mL of THF. After stirring for 2 h, the reaction mixture was cooled to −78 °C with dry ice, and 0.81 mL of 1,11-dibromoundecane was added. Subsequently, the mixture was stirred for 48 h and allowed to warm to room temperature. After filtration, the solvent was evaporated. The viscous residue was purified through a column filled with silica 60 and eluted with 10 vol % of ethyl acetate in petroether. A slightly yellow crystal solid (Br−Py) was collected and characterized by mass spectrometry and proton nuclear magnetic resonance (^1H NMR) as well as single-crystal diffraction. The yield was 64%.

Fifty (50) microliters of APS and 50 mg of Br−Py were added to 5 mL of toluene, and the reaction was catalyzed with 3 mL of Et_3N and 5 mg of $AgNO_3$. The reaction mixture was shaken for over 24 h, and the solvent was then removed by rotary evaporation. The residue was purified by column chromatography using silica 60 as a stationary phase and 10 vol % of ethyl acetate in hexane as the elution phase. The product separation was monitored with thin-layer chromatography (TLC). As the elution time of the APS−Py product was very close to that of the unreacted Br−Py material, they were not completely separated in the collected fraction. The fraction was then rotary evaporated, and the resulting solid residue was dissolved in a small amount of ethyl acetate. The solution was loaded on a large TLC plate. The APS−Py product was successfully separated with 5 vol % of ethyl acetate in hexane. The strip of the TLC plate containing the APS−Py was collected and eluted with pure ethyl acetate. After evaporating the solvent, the nearly white powder, APS−Py, was obtained.

Freshly prepared $Fe_xO_y@SiO_2$ nanoparticles with a shell thickness of about 10−15 nm were used for Py attachment. In particular, 3.6 mg of APS−Py was dissolved in 5 mL of 2-propanol and then mixed with 40 mL of the $Fe_xO_y@SiO_2$ dispersion. The mixture was

(15) Zhao, X.; Hillard, L. R.; Merchery, S. J.; Wang, Y.; Bagwe, R. P.; Jin, S.; Tan, W. *Proc. Natl. Acad. Sci. U.S.A.* **2004**, *101*, 15027.
(16) Santra, S.; Wang, K.; Tapec R.; Tan, W. *J. Biomed. Opt.* **2001**, *6*, 160.
(17) Stöber, W.; Fink, A. *J. Colloid Interface Sci.* **1968**, *26*, 62.
(18) Lu, Y.; Yin, Y.; Mayers, B. T.; Xia, Y. *Nano Lett.* **2002**, *2*, 183.

mechanically stirred at 60 °C for over 20 h. The as-synthesized Fe_xO_y@SiO_2−Py nanoparticles were precipitated with the addition of acetone and washed with water and 2-propanol several times to remove physisorbed APS−Py molecules on the particle surface. The washed particles were re-suspended in 2-propanol for optical characterization.

For comparison, we also attached the Py group to the surface of the as-received Fe_xO_y nanoparticles directly. Here, 3.6 mg of APS−Py was dissolved in 5 mL of 2-propanol and then mixed with 6 mL of the primary stock solution of Fe_xO_y and 43 mL of 2-propanol. To this mixture, 0.64 mL of NH_4OH was added under vigorous stirring. The reaction was allowed to proceed at 60 °C for over 20 h. The modified particles (Fe_xO_y−Py) were washed as described above for the Fe_xO_y@SiO_2−Py nanoparticles.

Characterization. Transmission electron microscopy (TEM), energy-dispersive X-ray (EDX) spectroscopy, and X-ray diffraction (XRD) were used for structural characterization for the as-received iron oxide nanoparticles and the Fe_xO_y@SiO_2 core−shell nanoparticles. Low- and high-resolution TEM images were obtained using a Philips CM20 FEG microscope operating at 200 kV. EDX spectra were collected from the core and the shell regions separately during TEM imaging. Samples were prepared by dropping several drops of the particle dispersion onto the grids with a pipet. Powder XRD measurements were performed at room temperature with a Scintag X_2 diffractometer equipped with a Cu Kα radiation source (λ = 0.154 nm). The patterns were obtained within the 2θ range of 20−70° in step mode with step size of 0.06° and collection time of 20 s. The profile was analyzed with the Pearson VII software after background subtraction and $K\alpha_2$ stripping. The average size of the as-received Fe_xO_y nanoparticles was estimated using the Scherer equation.

Both direct current (DC) and alternating current (AC) magnetic measurements were done using a Quantum Design PPMS model 6000 magnetometer. To measure the field-dependent DC magnetization, a field of 40 kOe was initially applied to the sample and gradually decreased to 0 followed by field reversal and gradual increase to −40 kOe. The magnetization measurements were carried out at a constant temperature of 300 K. DC magnetization was also measured as a function of temperature. In this case, the sample was cooled either in zero field (zero-field cooled, ZFC) or in the field (field cooled, FC) of 50 Oe from room temperature down to about 10 K. Then the sample was heated from 10 to 350 K in the 50 Oe field, and the magnetization data were recorded during this heating cycle. All the magnetization data were normalized to the sample weight. The sample was prepared by filling a gelatin capsule with magnetic powders, which was subsequently sealed with Parafilm.

UV−visible spectra were acquired with a Cary 5000 UV−vis−near-infrared spectrophotometer (Varian) with a scan speed of 300 nm/min. Emission spectra were measured with a C700 PTI system (Photon Technology International) equipped with a Xenon lamp using the excitation wavelengths of 450 nm for Rubpy and 270 nm for the Py groups.

Results and Discussion

The size distribution and the crystal structure of the as-received iron oxide nanoparticles have been characterized with TEM and XRD. From TEM observations, the particle size varies from a few nanometers to over 20 nm as seen in Figure 1. The wide particle size distribution is not unusual in the synthesis of metal oxide nanoparticles. For modeling work, it is critical to obtain particles with an accurate mean size and a narrow size distribution. As the aim of our work is to demonstrate the potential and efficiency of combining magnetic and luminescent functionalities into one architecture for practical applications, the particle size is not believed to be an important issue at this stage as long as the size of most particles does not exceed a critical value leading to the loss of superparamagnetism or causing other practical problems associated with particle size, for example, insufficient circulation time. As shown below, our nanoparticles exhibit superparamagnetic properties.

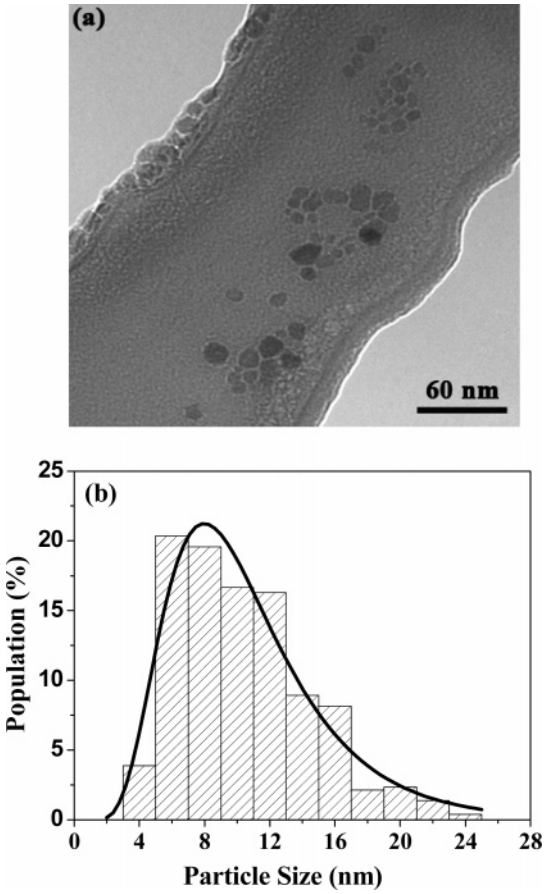

Figure 1. (a) TEM image of as-received Fe_xO_y nanoparticles and (b) size histogram along with curve fitting assuming log-normal distribution of the as-received Fe_xO_y nanoparticles.

The size distribution has been fitted with the log-normal equation,[19] and it yielded a mean particle size of 9.7 ± 0.4 nm (Figure 1b). Not all particles appear round, though; some of them are oval in shape. The crystal structure has been studied with powder XRD. The diffraction peaks and their relative intensities (Figure 2a) match well with those of γ-Fe_2O_3 and/or Fe_3O_4. These two crystal phases cannot be distinguished by XRD because of the same inverse spinel structure and similarity in their *d* spacing. However, because γ-Fe_2O_3 and Fe_3O_4 have similar magnetic properties, it is not necessary to identify the percentage of each phase. The average domain size has been estimated from the (311) reflection using the Scherer equation. The calculated value of 10.2 nm is rather close to that obtained from TEM observations, indicating that these nanoparticles are composed of single crystallographic domains and also are highly crystalline.

(19) Ngo, A. T.; Bonville P.; Pileni, M. P. *Eur. Phys. J. B* **1999**, *9*, 583.

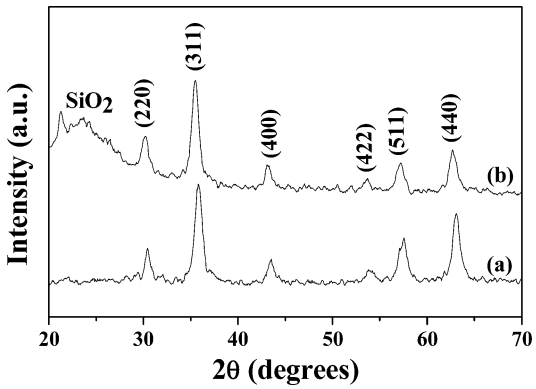

Figure 2. XRD patterns of (a) as-received Fe_xO_y and (b) $Fe_xO_y@SiO_2$ core−shell nanoparticles.

The $Fe_xO_y@SiO_2$ core−shell nanoparticles have been synthesized through a sol−gel approach. The shell thickness has been well-controlled by changing the TEOS concentration.[20] As shown in Figure 3a, the core−shell structure is obvious and well-resolved with TEM as a result of the good contrast between the core and the shell regions. Most of the particles have either a single core or double cores. The shell thickness is rather uniform, and the overall particle size changes with the core size. The surface roughness depends on the water and NH_4OH concentrations because changes in these concentrations lead to changes in the dielectric constant and ionic strength of the coating solution,[21] which in turn have complicated effects on the nucleation, growth, and agglomeration of the silica network. Figure 3b shows a representative core−shell particle with granular surface morphology. The presence of grains on the surface makes it difficult to identify the core−shell morphology. These grains could be mistaken for Fe_xO_y, but as shown in Figure 3d, EDX indicates that they are made of silica. Iron is only detected in the central region, which confirms that the core−shell architecture is formed and that the core is situated roughly in the center. The size of this particle is also larger than those from other samples because more TEOS has been used in this preparation. As illustrated in Figure 3c, smooth shells are formed by reducing the concentrations of water and NH_4OH in the coating dispersion. In the case shown, the amounts of pure water and NH_4OH were decreased from 32 to 20 mL and from 4 to 2.4 mL, respectively. XRD measurements were carried out on the samples with smooth shells. As shown in Figure 2b, the presence of amorphous silica is easily detected in the 20−35° regions as a broad featureless band.[22]

The magnetic properties of the $Fe_xO_y@SiO_2$ nanoparticles with a shell thickness of 10−15 nm have been measured and compared with those of the as-received Fe_xO_y nanoparticles. Figure 4a shows a quite different temperature dependence behavior for the two types of particles. All the curves have been normalized to their corresponding FC maxima. For the as-received Fe_xO_y nanoparticles, the ZFC maximum, that is, the generally defined mean blocking temperature (T_B), is slightly over 300 K. This value is significantly higher than that of the $Fe_xO_y@SiO_2$ nanoparticles, which show a ZFC maximum at 158 K. The reduction is mainly attributed to the decrease in the interparticle interactions due to the increase in the separation distance between the magnetic cores with the formation of the silica shells.[23] The weaker magnetic interactions in the $Fe_xO_y@SiO_2$ sample are indirectly reflected in the steeper slope of its FC curve below T_B.[24] By comparing our value of T_B for $Fe_xO_y@SiO_2$ with those reported in the literature for iron oxide nanoparticles,[25] one can conclude that the $Fe_xO_y@SiO_2$ nanoparticles are indeed only weakly interacting. This is also confirmed from our AC susceptibility study.[20] Besides the ZFC maximum, the bifurcation point between the ZFC and the FC curves, that is, the maximum T_B, for the $Fe_xO_y@SiO_2$ nanoparticles is well below room temperature and occurs at 198 K. This result indicates that the $Fe_xO_y@SiO_2$ nanoparticles are superparamagnetic at room temperature.

The hysteresis loops of the as-received Fe_xO_y and $Fe_xO_y@SiO_2$ nanoparticles measured at 300 K are shown in Figure 4b. Both of them exhibit negligible coercivity (H_c) and remanence, typical of superparamagnetic materials. This observation indicates that even though the as-received Fe_xO_y nanoparticles have the ZFC maximum slightly above 300 K, they still exhibit negligible coercivity and remanence. For systems with wide particle size distributions, it is known that the ZFC maxima usually overestimate the mean T_B.[26] Therefore, the true mean T_B of the as-received Fe_xO_y should be somewhat below 300 K. This would allow a large population of the Fe_xO_y nanoparticles to relax quickly with decreasing magnetic field at 300 K, thus leading to a small coercivity and remanence. Interestingly, the as-received Fe_xO_y and $Fe_xO_y@SiO_2$ samples exhibit the same "residual" H_c at 300 K, even though they show different T_B values. The small H_c of about 20 Oe in the $Fe_xO_y@SiO_2$ sample is readily attributable to the small fraction of particles with magnetic cores larger than 20 nm (see Figure 1b), which is the size threshold for non-superparamagnetic behavior,[27] and to the small fraction of particles which exhibit multi-core structures. Obviously, the large magnetic nanoparticles are also present in the as-received sample, and on account of stronger magnetic interactions one should expect a different H_c. But, the experiment indicates little if no change in H_c upon coating. The presence of some multi-core structures in the coated samples complicates the interpretation, as its effect on H_c cannot be quantified at present. Extensive magnetization data on several samples with different shell thicknesses as well as different dilution methods and at different temperatures would be required to provide further insights

(20) Ma, D.; Guan, J.; Normandin, F.; Veres T.; Kinston, D.; Simard, B. Superparamagnetic Core-Shell Nanostructure: Controlled Synthesis and Magnetic Characterization. In preparation.
(21) Mine, E.; Yamada, A.; Kobayashi, Y.; Konno, M.; Liz-Marzán, L. *J. Colloid Interface Sci.* **2003**, *264*, 385.
(22) Grasset, F.; Labhsetwar, N.; Li, D.; Park, D. C.; Saito, N.; Haneda, H.; Cador, O.; Roisnel, T.; Mornet, S.; Duguet, E.; Portier, J.; Etourneau, J. *Langmuir* **2002**, *18*, 8209.
(23) Vestal, C. R.; Song, Q.; Zhang, Z. J. *J. Phys. Chem. B* **2004**, *108*, 18222.
(24) Tronc, E.; Prene, P.; Jolivet, J. P.; d'Orazio, F.; Lucari, F.; Fiorani, D.; Godinho, M.; Cherkaoui, R.; Nogues, M.; Dormann, J. L. *Hyperfine Interact.* **1995**, *95*, 129.
(25) Vestal, C. R.; Zhang, Z. J. *Int. J. Nanotechnol.* **2004**, *1*, 240.
(26) Sappey, R.; Vincent, E.; Hadacek, N.; Chaput, F.; Boilot, J. P.; Zins, D. *Phys. Rev. B* **1997**, *56*, 14551.
(27) He, Y. P.; Wang, S. Q.; Li, C. R.; Miao, Y. M.; Wu, Z. Y.; Zou, B. S. *J. Phys. D: Appl. Phys.* **2005**, *38*, 1342.

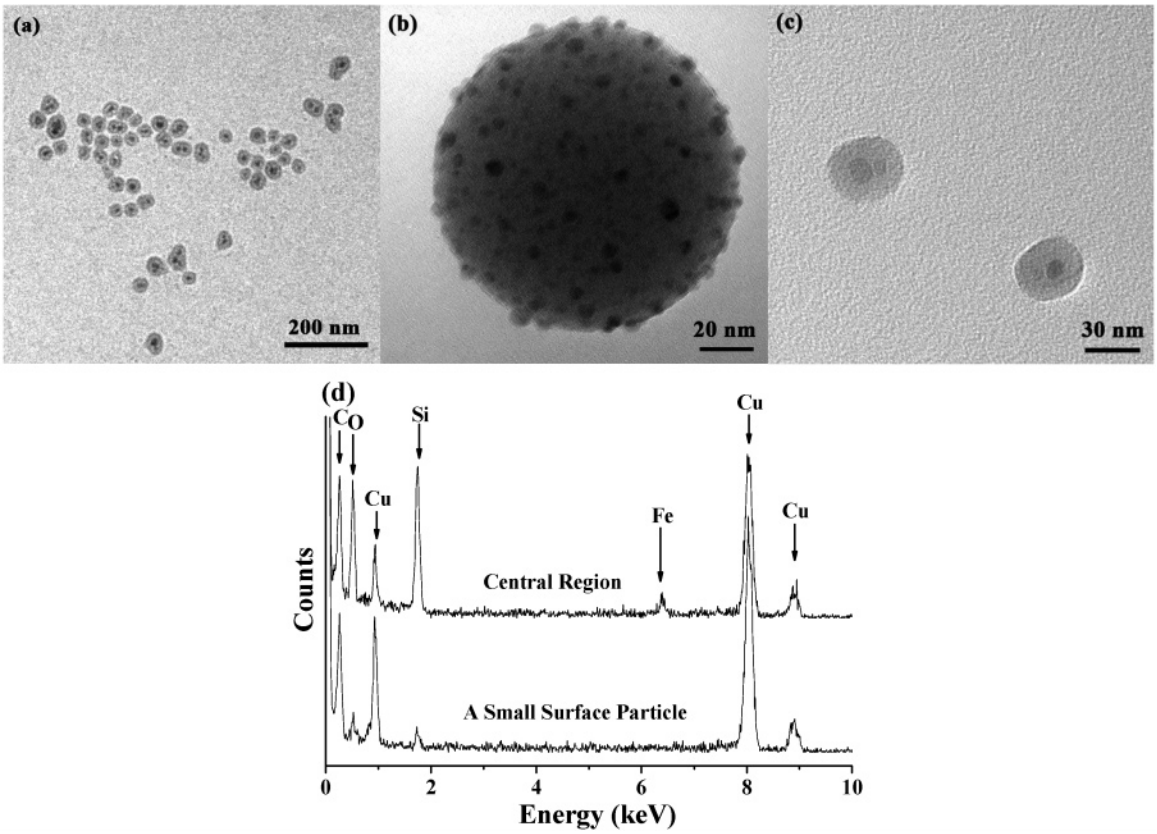

Figure 3. TEM images showing (a) a group of $Fe_xO_y@SiO_2$ core−shell nanoparticles and (b and c) $Fe_xO_y@SiO_2$ core−shell nanoparticles with different surface morphologies. The TEOS amount used for the synthesis of the particles in part a is 40 μL, and the other conditions are the same as those described in the experimental section. The H_2O, NH_4OH, and TEOS amounts used for the synthesis of the particle in part b are 32, 4, and 0.44 mL, respectively, and the other conditions are the same as those described in the experimental section. The particles in part c are prepared using the procedures described in the experimental section. (d) EDX spectra of the central region of a core−shell nanoparticle and a small surface particle.

into this interesting issue. These go beyond the scope of this paper.

The saturated magnetization of the $Fe_xO_y@SiO_2$ is smaller than that of the as-received Fe_xO_y, due to the presence of the nonmagnetic silica shell. Although the Rubpy-doped $Fe_xO_y@SiO_2$ nanoparticles are expected to have a further decreased magnetization, they are still magnetically useful. Within the scope of another study,[28] we have prepared Rubpy-doped Fe_xO_y $@SiO_2$ nanoparticles with a thicker silica shell of 40 nm and found that even with this shell thickness, the particles can be easily confined with small commercial magnets. But for the purpose of practical applications, superparamagnetic materials with as high a magnetization as possible are desired. Therefore, thinner silica shells are preferred as long as they are still thick enough to prevent luminescence quenching. To this effect we proceeded to synthesize a silica shell as thin as 10 nm. Before encapsulating dye molecules inside a second silica shell, Py molecules have been attached to the surface of the $Fe_xO_y@SiO_2$ nanoparticles with a single-shell thickness of 10−15 nm to determine whether fluorescence quenching by the magnetic cores can be avoided.

To attach the Py group covalently to the $Fe_xO_y@SiO_2$ surface, Br−Py was synthesized and then reacted with APS to form APS−Py. Br−Py has been identified with mass spectrometry, ^{1}H NMR, and single-crystal diffraction. In the mass spectrum, the parent ion is observed at 466. The observed shifts in the ^{1}H NMR spectrum in deuterated chloroform have been assigned as follows: 9H (d, 2t, m) from 8.5 to 7.9 ppm belonging to pyrene-H, 2H (s) at 5.24 ppm to pyrene-CH_2, 2H(t) at 3.63 ppm to CH_2−Br, 2H(t) at 3.41 ppm to O−CH_2, and 18H(m) from 2 to 1 ppm to the $(CH_2)_9$ chain of undecanyl. Single-crystal structure analysis yielded the unit cell data of $a = 8.6232(4)$ Å, $b = 9.2261(4)$ Å, $c = 28.4554(13)$ Å, $\alpha = 90°$, $\beta = 95.9880(10)°$, $\gamma = 90°$, and R1 = 0.0421 (see Supporting Information). The formation of APS−Py has been confirmed by mass spectrometry with the parent ion at 605 and ^{1}H NMR spectra (not shown here).

The APS−Py complex can be easily hydrolyzed and bound to the silica surface. In this process, the APS works as a bridge to link the Py group to the $Fe_xO_y@SiO_2$ nanoparticle surface. Emission spectra from Br−Py in cyclohexane and APS−Py, $Fe_xO_y@SiO_2$−Py, and Fe_xO_y−Py in 2-propanol have been recorded and are shown in Figure 5. Br−Py and APS−Py exhibit almost the same emission spectra regardless of the solvent used. The emission band becomes much broader after the Py is attached covalently on the $Fe_xO_y@SiO_2$ surface. A slight red shift is observed for $Fe_xO_y@SiO_2$−Py relative to Br−Py and APS−Py. Despite these slight differences, one can readily conclude that the Py fluorophores are not totally quenched by the iron oxide cores. In marked contrast, no emission is observed when the Py fluorophores

(28) Ma, D.; Simard, B. A New Approach towards Controlled Synthesis of Multifunctional Core-Shell Nano-Architectures: Luminescent and Superparamagnetic. *Nanotechnology*, submitted for publication.

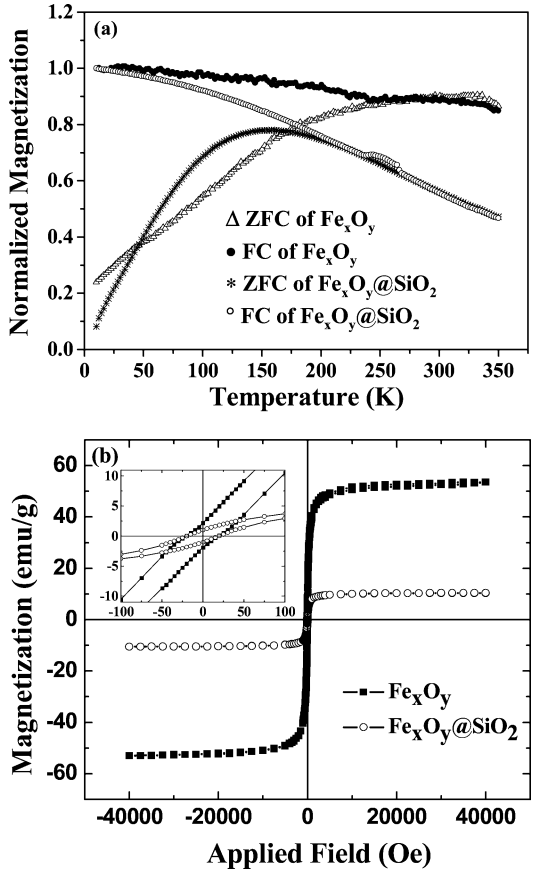

Figure 4. (a) Temperature dependence of the magnetization for the as-received Fe_xO_y and Fe_xO_y@SiO_2 core−shell nanoparticles and (b) hysteresis loops taken at 300 K for the as-received Fe_xO_y and Fe_xO_y@SiO_2 core−shell nanoparticles. The inset shows an expanded view of the low-field regions of the hysteresis loops.

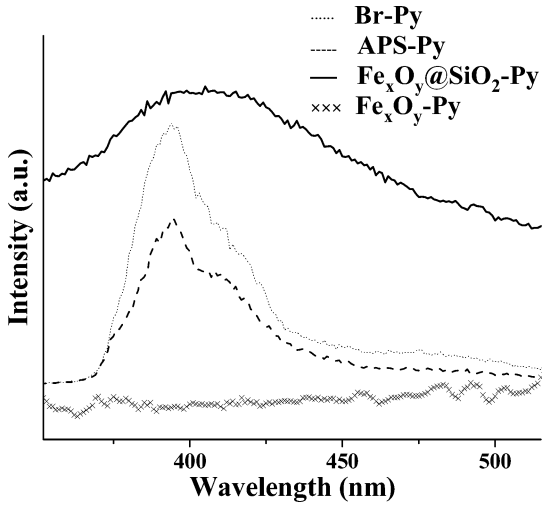

Figure 5. Emission spectra of Br−Py in cyclohexane (dotted line), APS−Py in 2-propanol (dashed line), Fe_xO_y@SiO_2−Py in 2-propanol (solid line), and Fe_xO_y−Py in 2-propanol (×).

are directly attached to the Fe_xO_y surface. On the basis of the above observations, one can conclude that a 10−15 nm silica shell is thick enough to insulate the fluorophore from the magnetic core and that the Fe_xO_y@SiO_2 nanoparticles are well-suited for the development of a "magnetic light bulb". Dye encapsulation in a second silica shell has been performed using the inorganic dye Rubpy rather than Py because of its better compatibility with the silica matrix.[29] In addition, for comparison, Rubpy-doped silica nanoparticles (no magnetic core) have also been prepared using a similar method.

Figure 6 shows TEM images of the Rubpy-doped silica and Rubpy-doped Fe_xO_y@SiO_2 nanoparticles. The sizes of the Rubpy-doped silica nanoparticles vary from 20 to over 100 nm. In general, pure silica particles with narrow size distributions can be synthesized with the traditional Stöber method. Here, the nonuniform size distribution is thought to be due to interference from the Rubpy in the particle nucleation and growth processes. The ionic concentration in the coating solution is increased, and the negative charge density on the particle surface is decreased with the introduction of Rubpy. Both factors directly affect the particle stability in the dispersion and subsequent silane condensation. The particles appear spherical, but some of them have irregular shapes with fluffy amorphous silica on their surfaces. The irregular surface morphology is again attributed to the introduction of Rubpy. By increasing the reaction time, a better surface morphology and more uniform size are obtained. The same strategy has been applied to the Fe_xO_y@SiO_2 nanoparticles. After Rubpy incorporation, in addition to the core−shell structures, some agglomerates and core-free silica nanoparticles, which can be removed by either centrifugation or magnetic extraction, are formed. The shell thickness has increased to around 25 nm. Therefore, the Fe_xO_y@SiO_2@SiO_2−Rubpy architecture has the comparable dye-free and dye-doped silica shells with average thicknesses a little over 10 nm per shell. We believe that the interactions between the magnetic cores totally disappear with this double-shell thickness and that effectively, the Fe_xO_y@SiO_2 nanoparticles act chemically like pure silica nanoparticles. The silica shell stabilizes the colloidal dispersion and also aids in particle redispersion after centrifugation. Unwanted morphologies, such as irregularly shaped agglomerates, have also been observed when Rubpy and TEOS were added quickly to the reaction dispersion. The observations indicate that the resulting morphology is very sensitive to the rate of reagent addition. By employing a slow, dropwise addition method, a much better morphology is produced.

UV−vis absorption and emission spectra of the free Rubpy, Rubpy-doped silica, and Rubpy-doped core−shell nanoparticles are shown in Figure 7. The free Rubpy in the aqueous medium exhibits an absorption band at 453 nm. The absorption becomes weaker with the Fe_xO_y@SiO_2@SiO_2−Rubpy architecture as a result of obvious scattering from large particles, magnetic cores, or agglomerates, which causes the absorption feature to be superimposed by a steadily increasing baseline. In contrast, the Rubpy-doped silica nanoparticles do not display this scattering effect because of the lack of agglomerates and the absence of a core−shell interface. They exhibit an absorption spectrum similar to that of the free Rubpy. The free Rubpy in the aqueous medium has an emission band at 608 nm. As Rubpy is doped inside the silica matrix, irrespective of whether the architecture is pure silica or silica shells, the emission feature neither shifts nor becomes broader (Figure 7b, inset). This suggests that

(29) Tapec, R.; Zhao, X.; Tan, W. *J. Nanosci. Nanotechnol.* **2002**, *2*, 405.

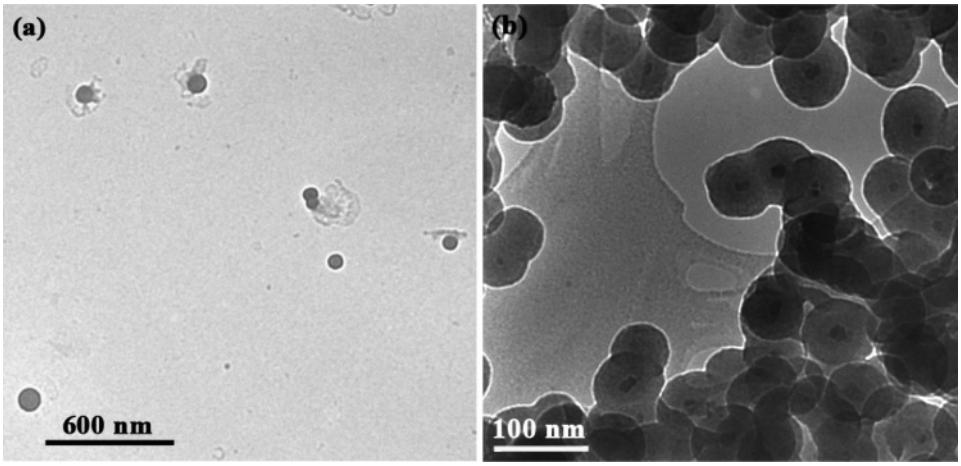

Figure 6. TEM micrographs of (a) Rubpy-doped silica nanoparticles and (b) Rubpy-doped core−shell nanoparticles (Fe_xO_y@SiO_2@SiO_2−Rubpy).

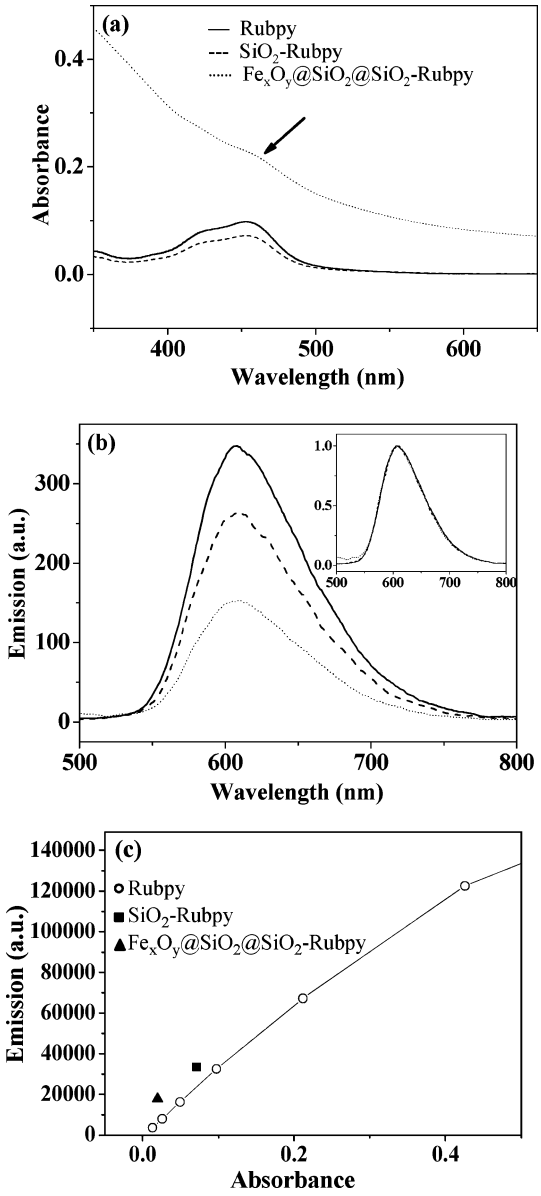

Figure 7. (a) UV−vis absorption spectra of, (b) emission spectra of, and (c) integrated emission intensity versus absorbance at 450 nm for Rubpy, Rubpy-doped silica nanoparticles, and Rubpy-doped core−shell nanoparticles (Fe_xO_y@SiO_2@Rubpy−SiO_2). The legend of part b is the same as that in part a. The inset in part b shows normalized emission spectra of the three samples.

the photophysical properties of Rubpy are not being altered when the Rubpy is embedded inside the silica matrix. Further evidence is provided through an examination of the emission intensities. Here, because it has not been possible to determine the concentrations accurately, the emission intensities are plotted against the absorbance at 450 nm, which is the excitation wavelength. Emission intensities have been calculated by integrating the peak area between 515 and 800 nm in the emission spectra. Scattering effects have been taken into account for the Fe_xO_y@SiO_2@SiO_2−Rubpy system, and its contribution to the 450 nm absorbance has been subtracted from the overall absorbance to get the net absorbance of the Rubpy at that wavelength. As seen in Figure 7c, the luminescence of Rubpy in the aqueous medium correlates with the 450 nm absorbance fairly linearly at low concentrations. The data points for Rubpy-doped nanoparticles are close to the emission-absorbance line for free Rubpy, and considering the experimental error, it can be safely concluded that the luminescence efficiency and, hence, the overall photophysical properties of the Rubpy are not affected significantly by the doping process. This means that the magnetic cores do not alter the photophysical properties of Rubpy which is notably due to the buildup of the first silica shell. A third silica coating may be done to further protect the dyes from photobleaching. The photostability as well as other photophysical properties of the nano-architecture will be investigated and reported in a subsequent paper.

Conclusion

A multifunctional nano-architecture containing superparamagnetic cores and dye-doped silica shells has been synthesized through a modified Stöber method. Magnetic measurements reveal that these nanoparticles exhibit improved superparamagnetic behavior with a significant decrease in the blocking temperature due to the absence of magnetic interactions. The architecture demonstrates similar emission properties as the free dye molecules, suggesting that the inner silica shell successfully screens the interaction between the dye and the magnetic core. The designed architecture not only enables the powerful combination of two useful functions, superparamagnetism and luminescence, but also allows highly sensitive detection because each

nanoparticle contains several thousands of dye molecules, thus yielding a "magnetic light bulb" entity of high brightness. Moreover, in this architecture, the silica surface remains available for versatile bioconjugation with a variety of probes. This multifunctional architecture can be used in many applications such as rapid diagnostics, phototherapies, and imaging technologies.

Acknowledgment. This work is supported by CBRN Research and Technology Initiative (CRTI) 03-0005RD. We gratefully thank Val Gertsman and Catherine Bibby for taking the TEM images. B.S. and D.M. are grateful to Dr. Kanchana Somaskandan for helpful discussion.

Supporting Information Available: X-ray crystal structure of 1-pyrenemethoxybromoundecane (Br−Py; PDF). An X-ray crystalographic file (CIF) for Br−Py. This material is available free of charge via the Internet at http://pubs.acs.org.

CM052067X